PHYSICAL REVIEW C, VOLUME 60, 064601

Positron-electron pairs produced in heavy-ion collisions

I. Ahmad,[1] Sam. M. Austin,[2] B. B. Back,[1] R. R. Betts,[1,3] F. P. Calaprice,[4] K. C. Chan,[5] A. Chishti,[6] C. M. Conner,[3] R. W. Dunford,[1] J. D. Fox,[6,*] S. J. Freedman,[1,7] M. Freer,[1,8] S. B. Gazes,[9,10] A. L. Hallin,[11] Th. Happ,[1,12] D. Henderson,[1] N. I. Kaloskamis,[5,†] E. Kashy,[2] W. Kutschera,[1] J. Last,[1] C. J. Lister,[1] M. Liu,[11], M. R. Maier,[8] D. M. Mercer,[2] D. Mikolas,[2] P. A. A. Perera,[9] M. D. Rhein,[1,12] D. E. Roa,[6,‡] J. P. Schiffer,[1,10] T. A. Trainor,[13] P. Wilt,[1] J. S. Winfield,[2,§] M. Wolanski,[1,10,∥] F. L. H. Wolfs,[9] A. H. Wuosmaa,[1] A. R. Young,[4] and J. E. Yurkon[2]

[1]*Physics Division, Argonne National Laboratory, Argonne, Illinois 60439*
[2]*NSCL and Department of Physics and Astronomy, Michigan State University, East Lansing, Michigan 48824*
[3]*Physics Department, University of Illinois at Chicago, Chicago, Illinois 60607*
[4]*Physics Department, Princeton University, Princeton, New Jersey 08544*
[5]*A. W. Wright Nuclear Structure Laboratory, Yale University, New Haven, Connecticut 06511*
[6]*Physics Department, Florida State University, Tallahassee, Florida 32306*
[7]*Lawrence Berkeley Laboratory, Berkeley, California 94720*
[8]*School of Physics and Space Research, University of Birmingham, P. O. Box 363, Birmingham B15 2TT, England*
[9]*Nuclear Science Research Laboratory, University of Rochester, Rochester, New York 14627*
[10]*Department of Physics, University of Chicago, Chicago, Illinois 60637*
[11]*Physics Department, Queen's University, Kingston, Ontario, Canada K7L 3N6*
[12]*Gesellschaft für Schwerionenforschung, Planckstrasse 1, D-64291 Darmstadt, Germany*
[13]*Nuclear Physics Laboratory, University of Washington, Seattle, Washington 98195*

(Received 25 November 1998; published 26 October 1999)

The production of positron-electron pairs in collisions of $^{238}U+^{232}Th$ at 5.95 MeV/nucleon, and of $^{238}U+^{181}Ta$ at 5.95, 6.1, and 6.3 MeV/nucleon, has been studied with the APEX spectrometer at Argonne National Laboratory. Several analyses have been performed to search for sharp structures in sum-energy spectra for positron-electron pairs. Such features have been reported in previous experiments. No statistically convincing evidence for such behavior is observed in the present data. [S0556-2813(99)06311-6]

PACS number(s): 25.70.Bc, 14.80.−j

I. INTRODUCTION

There is an extensive experimental and theoretical background to the study of positron production in collisions of very heavy ions, the essence of which is summarized in Refs. [1,2]. Briefly, it is expected that, when the combined charge of the target and projectile exceeds approximately 173, positron production associated with the overcritical binding of K-shell vacancies will occur. It was believed that attempts to isolate this so-called "spontaneous" production of positrons would be best carried out with the highest Z target and projectile combination, at an energy just below the Coulomb barrier, so that the competing background contribution of positrons from the internal-pair decay of states excited by nuclear processes would be minimized.

Pioneering experiments of this type were carried out at GSI-Darmstadt. The production of positrons in collisions of high-Z nuclei was indeed observed [3,4], with a continuous spectrum of energies centered at approximately 400 keV and a width of about 1 MeV. Analyses of these data showed that the observed positrons originated mainly from two sources: the internal-pair decay of excited states in the colliding nuclei, and from pairs produced by strong transient electromagnetic fields present in the collisions. The sought-for "spontaneous" positron production could not be isolated from the transient "dynamic" process.

Interest in these studies was heightened when unexpected narrow structures were observed [5–11] in the measured positron spectra. Similar structures were seen in a variety of collision systems. The widths of these features corresponded to the value expected from a monoenergetic source moving with approximately the center-of-mass velocity of the collision system. These observations led to a number of theoretical speculations, one of which was that the origin of the narrow positron lines was the two-body decay of a slowly moving neutral object into an positron-electron pair. The existence of such an object would require new physics, such as a new, light neutral elementary particle, or a novel narrow state of the positron-electron system. Such possibilities were, however, severely constrained by other results [12–17].

The suggestion of possible new physics prompted a new generation of heavy-ion scattering experiments to detect positrons and electrons in coincidence. Very sharp sum-energy peaks were found in the coincidence spectra, some of which appeared to possess the kinematic characteristics expected from the decay of a light, neutral object [18,19]. Subsequent

*Present address: Physics Division Oak Ridge National Laboratory P. O. Box 2008, Oak Ridge, TN 37831.

†Present address: Institute of Accelerating Systems and Applications, P.O. Box 17214, Athens 10024, Greece.

‡Present address: Advanced Photon Source, Argonne National Laboratory, Argonne, IL 60439.

§Present address: Department of Physics, University of Surrey, Guildford, Surrey U2 6RW, U.K.

∥Present address: Indiana University Cyclotron Facility, Bloomington, IN 47401.

TABLE I. Summary of experimental characteristics of previously reported e^+-e^- coincidence lines.

System	e^+-e^- sum energy (keV)	Line width (keV)	Beam energy (MeV/nucleon)	Energy loss in target (MeV/nucleon)	Cross section (μb/sr) (iso)[a]	(bb)[b]	Original reference
$^{238}U+^{232}Th$	608±8	25±3	5.86–5.90	0.07	2.7±0.6	1.1±0.3	[20,21]
$^{238}U+^{232}Th$	760±20	≤80	5.83	0.07	–	–	[18]
$^{238}U+^{232}Th$	809±8	40±4	5.87–5.90	0.07	3.1±0.7	1.3±0.3	[20,21]
$^{238}U+^{181}Ta$	625±8	20±3	6.24–6.38	0.10	3.2±0.8	1.3±0.3	[20,21]
$^{238}U+^{181}Ta$	748±8	33±5	5.93–6.13	0.10	5.7±1.3	2.3±0.5	[20,21]
$^{238}U+^{181}Ta$	805±8	27±3	6.24–6.38	0.10	3.3±0.8	1.4±0.4	[20,21]
$^{238}U+^{181}Ta$	≈635	≈30	6.30	0.24	0.5±0.1	–	[22]

[a]Cross section $d\sigma_{line}/d\Omega_{HI}$ calculated assuming isotropic angular correlation between positron and electron as presented in [23], except for $^{238}U+^{181}Ta$ 635 keV.

[b]Cross section $d\sigma_{line}/d\Omega_{HI}$ calculated assuming back-to-back positron-electron angular correlation as presented in [23].

experiments also revealed narrow sum-energy peaks, but with different energies in different collision systems, and without always fulfilling all the conditions for two-body decay [20–22]. Some evidence was also reported [20,21] for possible abrupt bombarding-energy dependence of the cross sections for peak production.

The lines in the positron spectra were observed at a level of a few percent of the total positron yield [8], corresponding to cross sections $d\sigma/d\Omega_{HI}\approx 5-10\mu$b/sr depending upon the range of heavy-ion detection angles. The positron-electron sum-energy lines were initially reported [18,20] to have yields consistent with those expected if the coincidence lines were produced with the same probability as the singles lines, but the most recent analyses of these data [23] gave values which were somewhat smaller. The values of the cross sections from several previous experiments as derived by Ganz *et al.*, as well as results reported in Ref. [9], are summarized in Table I.

At the time that the present work started, the above results represented an intriguing but puzzling body of observations that clearly merited further study. To this end, new experiments were carried out at GSI [23,24] and Argonne National Laboratory [25] to study this phenomenon, none of which have reported any evidence of sharp lines. This paper presents a report of the results from one of these new experiments—APEX (the ATLAS positron experiment), some of which have been reported previously [25–28]. In particular, we include an expanded discussion of the details of various analyses which were used to search for positron-electron pair lines as described in Letter form in Ref. [25]. Details of the APEX experiment particularly important for the data analysis are given in Sec. II. The general aspects of the various analyses are presented in Sec. III, and the results of specific analyses are presented in Sec. IV. Upper limits for peak cross sections derived from the two-body decay hypothesis and from the more empirically based analyses reported in the earlier work are given. An analysis of APEX data suggesting positive evidence for peaks has appeared [29]; the significance of this result is discussed. A discussion of our results appears in Sec. V, in which issues such as beam-energy and target-thickness dependence of the peak cross sections are covered.

II. EXPERIMENTAL APPARATUS

The central element of the APEX spectrometer is a large volume solenoid with a uniform 0.03 T magnetic field oriented perpendicular to the beam direction. Positrons and electrons produced in heavy ion collisions at the center of the solenoid are transported away from the target in helical trajectories and are detected in two segmented arrays of silicon PIN diode detectors placed on the solenoid axis. These detectors, which are 1 mm thick, record the kinetic energies of the positrons and electrons. To identify positrons which annihilate in these detectors, each silicon array is surrounded by a barrel-shaped assembly of NaI(Tl) crystals that detect the characteristic annihilation photons. To intercept direct photons emanating from the target, and suppress the large flux of low-energy electrons produced in the heavy-ion collisions, two conical, heavy-metal alloy shields (“electron/gamma stops”) are suspended on the solenoid axis on either side of the target. Scattered heavy ions are detected in an array of counters that provide the full azimuthal range. Finally, several different auxiliary detectors are used to monitor the target condition and incident beam flux. A detailed description of the APEX experimental apparatus appears in Ref. [30].

Possible positron events are first signaled by the APEX trigger processor [31] which analyzes the geometry of hits in the NaI(Tl) arrays and requires that the angle between two of the detected photons be in the range $165°\leq\phi_{\gamma\gamma}\leq 180°$. No requirement is made on the energy of the photons other than that they fire the discriminators in the trigger processor. Without beam, a trigger rate of about 40 Hz in each NaI(Tl) array arises from radioactivity in the concrete of the walls and floor of the target room and from cosmic-ray muons. With a ^{238}U beam of intensity 4 pnA incident on a 1 mg/cm^2 ^{181}Ta target, the residual radiation from the beam dump contributes an additional trigger rate of approximately 20 Hz in each array. By comparison, the actual rate of pos-

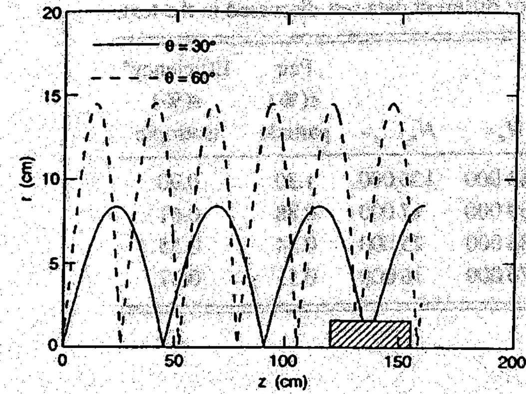

FIG. 1. Schematic illustration of the lepton polar angle measurement in APEX. In this example, a lepton with a kinetic energy of 400 keV is emitted at an angle of 30° (solid curve) and 60° (dashed curve) with respect to the solenoid axis, executing three and five cyclotron oscillations, respectively, in the magnetic field B before being detected a distance z along the solenoid axis, away from the target. The shaded bar indicates the extent of the silicon array.

itrons annihilating in one of the silicon arrays is only about 1 Hz. The requirement of a prompt time coincidence between the signals from the silicon and NaI(Tl) arrays, and the beam pulse, together with reconstruction of the origin of the annihilation radiation, results in positron spectra that contain fewer than 5% of events arising from misidentified electrons.

A feature of the APEX spectrometer is the ability to measure the emission angles of positrons and electrons. This determination is achieved through a combination of energy, time-of-flight, and position measurements, as illustrated in Fig. 1. A lepton emitted with energy E and polar angle θ, follows a unique helical trajectory in the magnetic field. From the measured energy and flight time of the lepton, and the distance between the target and the struck detector element, the total momentum p and its component along the solenoid axis (p_z) may be determined. The polar emission angle is then given by $\theta = \cos^{-1}(p_z/p)$. In principle, if the time resolution of the silicon detectors is smaller than the cyclotron period, the number of turns executed by the lepton along its trajectory may be uniquely determined, and the flight time is then the product of the number of turns times the cyclotron period, which depends only on E. In that case, the polar emission angle is determined to a resolution limited by the length of one element of the silicon detector array. The emission angles thus obtained may then be used, e.g., to perform kinematic corrections, or to calculate the invariant mass of positron-electron pairs.

A. Spectrometer acceptance and performance

The acceptance and performance of the APEX spectrometer for positrons and electrons have been evaluated with a variety of radioactive sources, as well as detailed Monte Carlo simulations of the apparatus using the code GEANT. These measurements and simulations are described in detail in Ref. [30]. APEX accepts positrons and electrons that are emitted at angles between 20° and 70° with respect to the solenoid axis. This range corresponds to emission angles between $20° < \theta_{beam} < 160°$, where θ_{beam} is the angle of emission with respect to the beam direction. This range has good overlap with the acceptance of the previous experiments [25,30].

The full-energy acceptance profile of APEX for both positrons and electrons is roughly bell shaped with a maximum near $E_{e^+}, E_{e^-} = 400$ keV, and falling to zero below 115 keV and above 1050 keV. In the ideal case, the maximum value of the detection efficiency is approximately 25% for electrons, and near 6% for positrons. This difference between positrons and electrons reflects the efficiency of the NaI(Tl) annihilation radiation detectors. Also included in this difference are the effects arising from choices made in the analysis of the annihilation photon data as described below. These choices were fixed in all analyses and their effects taken into account in the Monte Carlo simulations of the performance of the apparatus, as described in Ref. [30].

In practice, the precise values of the positron and electron efficiencies for a given measurement are affected by the number of functioning detectors (see below). The experimental values of the maximum positron and electron efficiencies at 400 keV were 4.5% and 18%, respectively, for the data set obtained for $^{238}U + ^{232}Th$ scattering.

The average energy resolution of the silicon detectors was 12 keV full width at half maximum (FWHM). Variations of the system resolution during the measurements were monitored on a regular basis using sources and pulsers. Only those silicon detectors maintaining an energy resolution better than 20 keV (FWHM) were included in the subsequent data analysis. Typically, this was the case for approximately 80% of the total number of detectors. This effect was also included in the Monte Carlo simulations of the detection efficiency for each measurement. The effect of nonworking silicon detectors upon the spectrometer acceptance depends sensitively upon their location in the silicon arrays. For the typical case of 80% working silicon detectors, the overall positron detection efficiency was reduced by approximately 30%.

The APEX positron-electron pair coincidence detection efficiency was studied using internal pair conversion (IPC) pairs from the 1.761 MeV 0^+ state in ^{90}Zr populated through the 0.0115% branch in the β^- decay of ^{90}Y. The measured full-energy efficiency for this IPC pair is $0.29 \pm 0.01\%$, in good agreement with the calculated value of $0.28 \pm 0.02\%$, where the uncertainties in each case are purely statistical [30]. For the hypothetical situation of positron-electron pairs resulting from the decay of a slow-moving neutral object with a mass of 1.8 MeV/c^2, with the positron produced isotropically in the emitter frame, the full sum-energy peak efficiency is larger due to the equal-energy and back-to-back angular correlations for the pair, and ranges between 0.55% and 1.3% depending on the set of detectors used. If the positron-electron pair has an isotropic angular correlation, the detection efficiency is reduced, and is between 0.37% and 0.90%. These values are summarized in Table II.

B. Heavy-ion detection

Scattered heavy ions were detected in an array of eight low-pressure multi-wire proportional counters (LPMWPC)

TABLE II. APEX integrated luminosities and pair efficiencies for different data sets discussed in the text.

System	Beam energy range[b] (MeV/nucleon)	Average target thickness (μg/cm^2)	Integrated luminosity (μb^{-1})	N_{e^+}	$N_{e^+e^-}$	Pair ϵ(%) particle	Efficiency[a] ϵ(%) isotropic
^{238}U+^{232}Th	5.78–5.95	760	7000	246 000	126 000	1.30	0.90
^{238}U+^{181}Ta	5.79–5.95	660	5800	59 000	17 000	0.88	0.61
^{238}U+^{181}Ta	5.94–6.10	650	11 000	84 000	25 000	0.84	0.55
^{238}U+^{181}Ta	6.13–6.30	700	8600	70 000	16 000	0.55	0.37

[a]Efficiency calculated for a pair line with sum energy of 778 keV.
[b]Beam energy range includes energy loss in the target.

[32]. These counters subtend polar angles with respect to the beam of 20° to 70°, and the entire 2π azimuthal range. Each detector is subdivided into three azimuthal sections, so the azimuthal scattering angle ϕ_{HI} is determined to $\pm 7.5°$. The dead spaces between counters and between different segments of each counter amount to approximately 10% of the solid angle. Each heavy-ion detector segment is position sensitive in the polar coordinate, and a timing signal from the LPMWPC anode is used to measure the flight time of the ions.

The intrinsic polar-angle (θ_{HI}) resolution of the counters is better than 0.5 degrees (FWHM), and the time resolution better than 0.5 ns (FWHM). The time-of-flight (TOF) and scattering-angle are used to determine the masses of the detected particles, assuming two-body scattering. The mass resolution obtained from this procedure is approximately 15 units for $A \approx 200$, and the Q-value resolution is approximately $\Delta Q \approx 25$ MeV.

For particles incident upon the active face of the heavy-ion counters, the detection efficiency for a single heavy ion is approximately 90%, averaged over the angle range subtended by the counter. The efficiency for detecting two coplanar heavy ions in coincidence is approximately 80% of that for a single ion in the ideal case when all counters in the array were operational. In the actual experiment, two ion detection also requires pairs of counters separated by 180 degrees in ϕ to be working simultaneously, which was not always the case. The heavy-ion pair-detection efficiency for the ^{238}U+^{232}Th data set was 74%, and ranged from 61% to 74% for ^{238}U+^{181}Ta. To be consistent with previous experiments, only events in which two identified heavy ions were present were retained in the analysis.

C. Beam and target monitoring and normalization

The experiments were carried out using ^{238}U beams of intensity between 2 and 4 pnA, with energies between 5.95 MeV/nucleon and 6.3 MeV/nucleon. The absolute beam energy was measured to a precision of approximately 0.025 MeV/nucleon using a time-of-flight system [33]. These beams were incident on rolled metal foils of ^{232}Th and ^{181}Ta of areal densities between 600 μg/cm^2 and 800 μg/cm^2. The foils were mounted on a rotatable target wheel, so that beam-induced damage could be spread if necessary. The Th target wheel was rotated at 300 rpm. The more robust Ta foils were not rotated, except to change the beam spot location every few hours. Information on the targets used and the integrated luminosity for the experiments discussed here are provided in Table II, and in Refs. [34,35].

The incident beam flux, the time structure of the beam, and the condition of the targets were monitored throughout the experiment. Two ionization chambers (ICs) were positioned in the vertical plane at 11 degrees relative to the beam direction. One of these ICs had a parallel-plate avalanche counter (PPAC) in front to measure the time structure of the beam. The energy resolution of the IC without the PPAC was approximately 0.5% for 6.1 MeV/nucleon ^{238}U. The position, shape, and integrated yield of the peak from the elastically scattered beam measured in this counter provided information on the target condition. If the rate of peak counts relative to the incident beam flux diminished or if the location of the peak centroid moved to lower energies (indicating thinning of the target) or broadened (indicating the onset of nonuniformity), the target was changed. In practice, targets were changed if the IC count rate changed by more than 10%. The integrated peak yields from each IC, the integrated beam current, and the IC solid angle were combined to determine the luminosity for each data set [35], assuming Rutherford scattering cross sections. The target thicknesses were obtained from measurements of the beam energy loss and from the measured elastic scattering yields.

Other monitor counters were also used. Two CsI detectors at 11 degrees on either side of the beam in the horizontal plane detected elastically scattered beam particles. These detectors provided additional checks on the target condition and beam intensity, and also ensured that the beam spot was centered on the target. Finally, two high-purity Ge detectors were used to detect photons emitted in the collisions. The data from these Ge detectors, after kinematic reconstruction, were used to determine the gamma-ray spectrum from the excited targetlike or projectilelike ions.

III. ANALYSIS

A. Positron identification

As noted above, positrons constitute a fraction of the trigger events. Most of the background is rejected during data analysis by the requirement of a prompt time coincidence between signals from the NaI(Tl) barrel and from the corresponding Si array. The conditions used to select these coincidences are shown in Fig. 2. The smaller peak in Fig. 2(b)

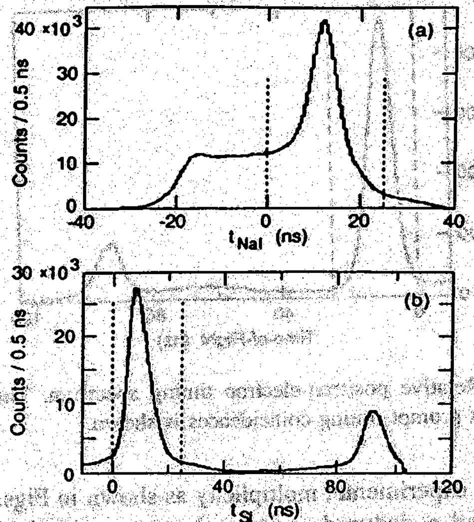

FIG. 2. Coincidence timing spectra for events with hits in both the NaI(Tl) and silicon detector arrays. (a) Timing of hits in the NaI(Tl) array with respect to the beam RF. (b) For events in the indicated region in (a), timing spectrum for hits in the silicon detector array relative to accelerator RF. The dashed lines indicate the limits of the windows for accepted events.

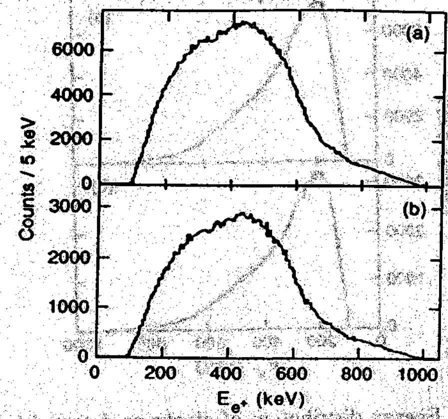

FIG. 4. (a) Energy distribution of positrons produced in the $^{238}U+^{232}Th$ reaction. No positron-heavy-ion coincidence is required. (b) Same as (a) except that two heavy ions are required to be detected in time coincidence with the positron.

arises from events from a neighboring beam burst, and the separation of 82 ns between the two peaks in this spectrum reflects the time structure of the ATLAS beam.

The identification of a valid positron also requires that at least one of the two photon signals must lie in the photo peak, and that there be a good correlation between the origin of the annihilation radiation, z_{NaI}, and the position of a hit on the silicon detector array, z_{Si}, where z is the distance from the target along the solenoid axis. All of the analyses presented here, including those from which the detection efficiency is determined, represent events which, in addition to containing photons which are detected in NaI crystals separated by approximately 180°, satisfy $|z_{Si}-z_{NaI}|\leq 5$ cm, as shown in Fig. 3.

The energy distribution of positrons thus identified from the $^{238}U+^{232}Th$ measurement is shown in Fig. 4. The contribution to this spectrum from misidentified electrons is less than 5%, and is largely confined to energies below 200 keV, as would be expected from the shape of the electron spectrum which is strongly peaked at low energies. The spectrum shown in Fig. 4(a) does not require a positron-heavy-ion coincidence, while that appearing in Fig. 4(b) requires that two heavy ions be detected in time coincidence with the positrons. The shapes of these two spectra are similar, indicating that most particles identified as positrons arise from valid heavy-ion collisions, and not from backgrounds unrelated to the beam.

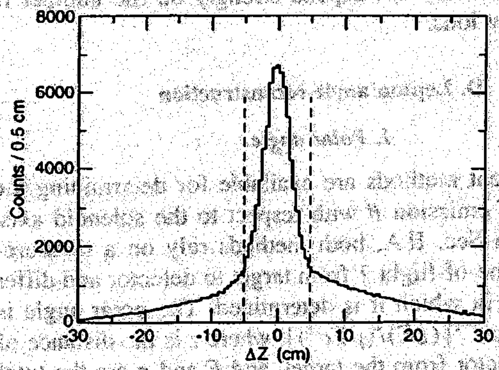

FIG. 3. Positron-identification spectrum showing the correlation in position between the reconstructed annihilation position from events in the NaI(Tl) barrel and hits in the corresponding silicon array. The dashed lines indicate the limits of the window for accepted events.

B. Electron multiplicity

The rate of electrons which fall inside the acceptance of APEX is 10^5 to 10^6 times greater than the positron rate. Therefore, all hits on the silicon arrays, other than those corresponding to identified positrons, are assumed to be electrons. Their energy distribution is consistent with that expected from the shape of previously measured spectra of atomic electrons [36] folded with the APEX response. Examples of electron spectra measured in coincidence with positrons emitted during $^{238}U+^{232}Th$ collisions are shown in Fig. 5. The fall-off below 200 keV is a consequence of the APEX acceptance, but above 200 keV the shape largely reflects the actual shape of the electron spectrum.

In $^{238}U+^{232}Th$ collisions near the Coulomb barrier, with heavy ions detected in the range $20°<\theta_{HI}<70°$, the multiplicity of electrons of energy above 100 keV has been measured to be between 4 and 5 [36]. Therefore, frequently more than one detected electron accompanies the detected positron resulting in multiple hits in the silicon arrays. Also, a lepton may backscatter and possibly deposit energy in more than one silicon wafer, but the probability of this occurring is at most 15%. Furthermore, the energy possessed by the backscattered particle is generally small and the resulting signal usually does not surpass the discriminator threshold and produce a hit in the silicon array.

The response of APEX to such multiple electrons has been studied using Monte-Carlo simulations. Figure 6(a) shows the calculated distribution of n-fold silicon detector

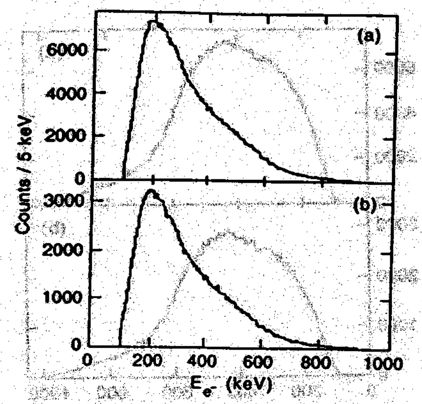

FIG. 5. (a) Energy distribution of electrons detected in coincidence with positrons for the $^{238}U+^{232}Th$ reaction. No electron-heavy-ion coincidence is required. (b) Same as (a) except that two heavy ions are required to be detected in time coincidence with the lepton pair.

hits (the silicon "fold" distribution), obtained from Monte-Carlo simulations of events with 1, 5, and 10 electrons produced per event, with an energy spectrum consistent with that of delta electrons. The measured fold distribution for $^{238}U+^{232}Th$ was used with these calculated distributions to estimate the experimental multiplicity as shown in Figs. 6(b) and 6(c), and a deduced average electron multiplicity for positron producing collisions of approximately 5 per collision was found, consistent with the results of the previous measurements [36].

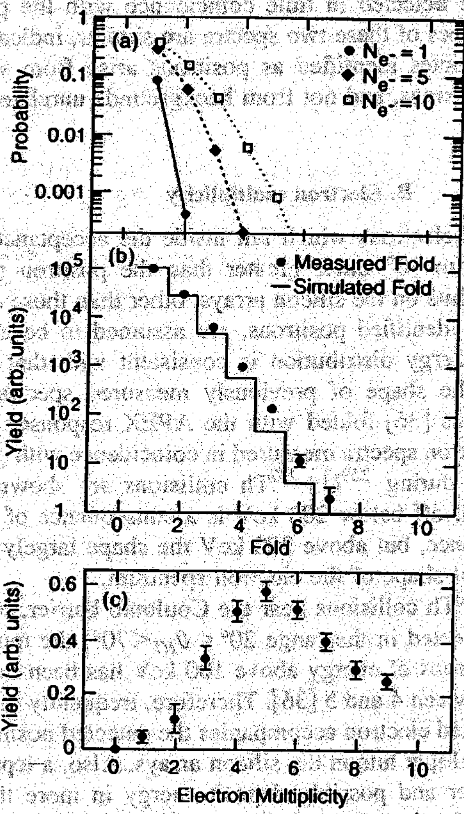

FIG. 6. (a) Calculated silicon fold distributions for events with electron multiplicities of $N_{e^-}=1$, 5, and 10. (b) Silicon fold measured for $^{238}U+^{232}Th$ collisions (data points.) The solid line represents a simulation of the expected fold distribution for the distribution of multiplicity shown in (c). (c) The electron multiplicity distribution obtained by deconvoluting the measured silicon fold distribution using the results of Monte Carlo simulations.

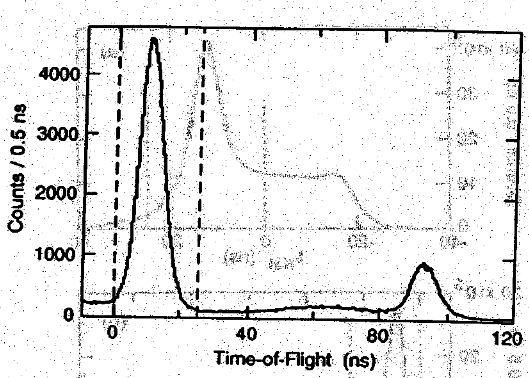

FIG. 7. Relative positron-electron timing spectrum. The gate used to select prompt timing coincidences is shown.

C. Positron-electron sum-energy distributions

True positron-electron pair events are selected by requiring that at least one electron be detected in prompt time coincidence with the positron. A spectrum of the relative flight time is shown in Fig. 7. The majority of the detected electrons are in prompt time coincidence with positrons; the window used to select these prompt events is shown. Random coincidences are also evident, arising from positrons and electrons from adjacent beam bursts. These random coincidences were used to estimate the contribution of uncorrelated positron-electron pairs in the prompt spectra.

As more than one detected electron frequently accompanies the detected positron, each positron-electron combination in a single event is treated as an independent pair, and the sum-energy spectra are incremented accordingly. Examples of sum-energy spectra from $^{238}U+^{232}Th$ collisions are shown in Fig. 8 for pairs both with and without a requirement on the number of detected heavy ions. As was the case for the individual positron and electron spectra, the shape of the distribution does not depend strongly on the number of detected heavy ions.

D. Lepton angle reconstruction

1. Polar angle

Two different methods are available for determining the polar angle of emission θ with respect to the solenoid axis. As outlined in Sec. II A, both methods rely on a measurement of the time-of-flight T from target to detector and differ in the manner in which it is determined. The polar angle is given by $\theta=\cos^{-1}[(zE)/(pTc^2)]$, where z is the distance of the struck detector from the target, and E and p are the total energy and momentum. In the APEX spectrometer, the lepton orbits have an integral number of turns and therefore, $T=NT_{cyc}$, where $T_{cyc}=(2\pi E)/(eBc^2)$, e is the charge, B is the strength of the magnetic field, and N the number of turns, leading to $\theta=\cos^{-1}[(z/p)\times(eB)/(2\pi N)]$.

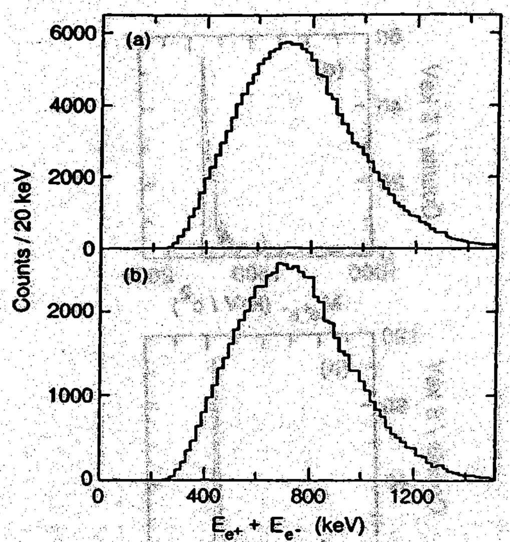

FIG. 8. (a) Sum-energy distribution of electrons and positrons detected in prompt time coincidence for the $^{238}U + ^{232}Th$ reaction. No lepton-heavy-ion coincidence is required. (b) Same as (a) except that two heavy ions are required to be detected in time coincidence with the lepton pair.

If the time-of-flight resolution ΔT is less than T_{cyc} (≈ 2 ns), the integer N may be determined from T and θ to a precision limited only by that of z and $p(E)$. For larger values of ΔT this method can still be used, but the precision is now limited by the number of events with miscounted turns and is no better than using the time-of-flight directly. In practice, the angular resolution obtained is limited by multiple scattering in the target and, as illustrated in Fig. 9, the particular choice of reconstruction method is of little consequence to the resolution.

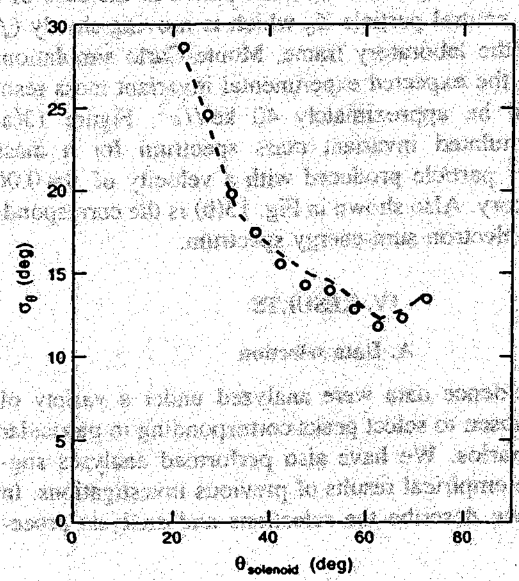

FIG. 9. Calculated resolution of the reconstructed polar emission angle as function of the emission angle for 400 keV electrons, calculated assuming a time-of-flight resolution of 4 ns, with multiple scattering in a 1000 mg/cm^2 Ta target, for continuous (symbols) and discrete (dashed line) time-of-flight.

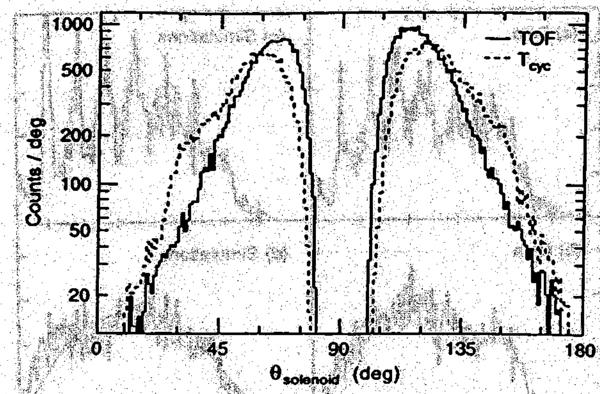

FIG. 10. Measured polar angular distributions for positrons produced in the $^{238}U + ^{232}Th$ reaction, obtained using the two angle reconstruction techniques discussed in the text.

In the measurements described in this paper, the energy-dependent time-of-flight resolution was larger than the cyclotron period and we calculate the polar emission angles using the time of flight directly. Reconstructed polar angle distributions for positrons produced from $^{238}U + ^{232}Th$ collisions with the two angle reconstruction techniques discussed above are shown in Fig. 10.

2. Azimuthal angle

The azimuthal emission angle (ϕ) is obtained from the azimuthal position of the struck silicon-detector element. The silicon arrays are divided into 18 segments in ϕ; in order to avoid anomalies that might be introduced in the analysis by discrete values of ϕ separated by 20°, the ϕ angles were smeared randomly by $\pm 10°$ over the range subtended by each element. An alternative method would be to not randomize ϕ, but rather to assign the value corresponding to the center of the silicon element. The consequences of the two methods of angle reconstruction are discussed in more detail below. Finally, a θ dependent correction to ϕ arising from the finite radial size of the silicon array was also included.

3. Pair opening angle

For positron-electron pairs, the opening angle θ_{+-} is calculated from the measured angles for the positron (θ_+, ϕ_+) and electron (θ_-, ϕ_-), and is given by $\cos\theta_{+-} = \sin\theta_+ \sin\theta_- \cos(\phi_+ - \phi_-) + \cos\theta_+ \cos\theta_-$. The reconstructed opening-angle distributions are significantly affected by the choice of reconstruction procedure used. In particular, the use of a discrete distribution in ϕ introduces artificial narrow structure in the opening angle correlations. This effect is illustrated in Fig. 11 which shows measured and simulated opening-angle distributions obtained using different methods of angle reconstruction. The source angular distribution in the simulation was isotropic. The simulated opening angle distribution for pairs accepted within the APEX acceptance, without the effects of multiple scattering or angle reconstruction is given by the solid line in Fig. 11(d).

E. Kinematic corrections and invariant mass distributions

Simulations show that the angular resolution in APEX is sufficient to allow kinematic correction of the energies of

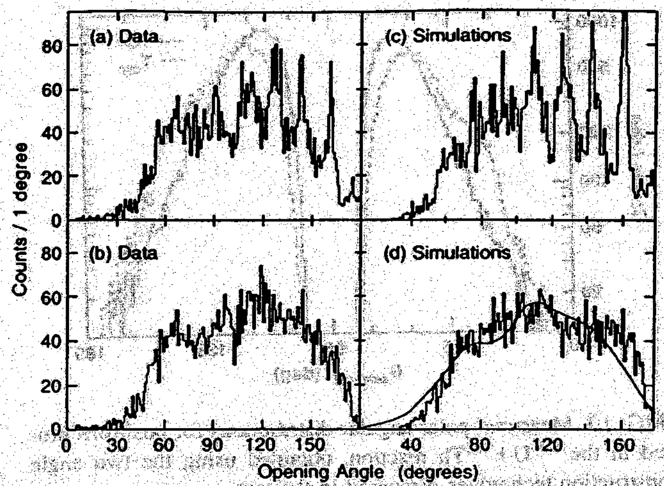

FIG. 11. Reconstructed opening-angle distributions for positron-electron pairs calculated with (a) discrete time of flight and ϕ, and (b) continuous time of flight and ϕ. (c),(d) Simulated opening-angle distributions for positron-electron pairs with $E(e^+)=E(e^-)=400$ keV, isotropic positron emission, and an isotropic opening-angle distribution. The curve in (d) represents the opening-angle distribution of pairs emitted into the APEX acceptance without the effects of multiple scattering.

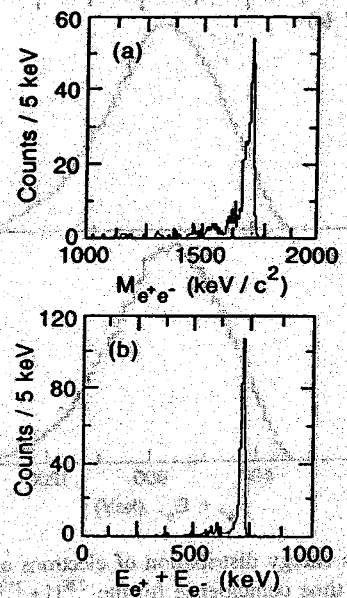

FIG. 13. (a) Simulated invariant-mass spectrum for a hypothetical particle X_0 with mass $M_{X_0}=1722$ keV/c^2. (b) Corresponding simulated positron-electron sum-energy spectrum.

internal conversion electrons emitted from moving ions with a resolution of 25 keV and of IPC pairs with a sum-energy resolution of 35 keV, when the velocity of the source is near 0.05c [27,37,38].

A demonstration of our ability to achieve these values is illustrated in Fig. 12, which shows kinematically corrected pair sum-energy spectra from IPC of a known 1.84 MeV $E1$

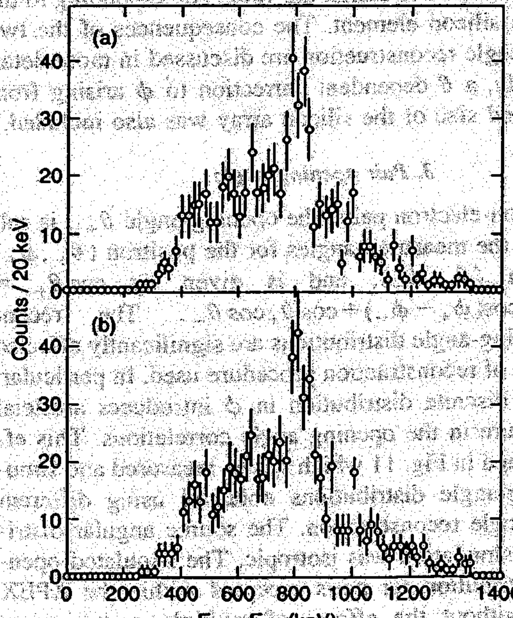

FIG. 12. Doppler corrected positron-electron sum-energy spectra from ^{206}Pb+^{206}Pb collisions, where the positron and electron angles have been calculated using (a) discrete time of flight and ϕ, and (b) continuous time of flight and ϕ.

transition in ^{206}Pb, excited in ^{206}Pb+^{206}Pb collisions at 5.90 MeV/nucleon [27]. In this analysis the angles were calculated using each of the methods described above. A selection on pair opening angle was imposed to enhance the signal according to the small-opening-angle peaking of the $E1$ IPC angular correlation. Within statistics, the two spectra are identical, and the peak due to the IPC transition is clearly apparent in both.

A similar situation is encountered in the calculation of the invariant mass of a positron-electron pair. For the case of a hypothetical neutral particle X_0 which is moving slowly ($\beta<0.05c$) in the laboratory frame, Monte-Carlo simulations indicate that the expected experimental invariant mass resolution would be approximately 40 keV/c^2. Figure 13(a) shows a simulated invariant mass spectrum for a mass 1722 keV/c^2 particle produced with a velocity of $\beta=0.06$ in the laboratory. Also shown in Fig. 13(b) is the corresponding positron-electron sum-energy spectrum.

IV. RESULTS

A. Data selection

The coincidence data were analyzed under a variety of conditions chosen to select peaks corresponding to particular physical scenarios. We have also performed analyses suggested by the empirical results of previous investigations. In this section we describe the selections and analysis procedures.

1. Energy selection

One class of selection is based on the electron and positron energies. If previously observed sharp sum-energy lines arise from the pair decay of a neutral object, in the rest frame of the source the energies of the positrons and electrons are

TABLE III. "Wedge-cut" parameters used in the data analysis. Wedge cuts are parametrized by $W_{\text{low}} \times E_{e^+} \leq E_{e^-\text{accepted}} \leq W_{\text{hi}} \times E_{e^+}$, as given in Refs. [18,20,22].

System	Beam Energy (MeV/nucleon)	Wedge cut	W_{low}	W_{hi}
$^{238}U+^{232}Th$	5.95	W1	0.67	1.50
$^{238}U+^{232}Th$	5.95	W2	0.75	1.25
$^{238}U+^{232}Th$	5.95	W3	0.68	1.25
$^{238}U+^{181}Ta$	5.95	W1	0.57	1.64
$^{238}U+^{181}Ta$	6.10	W2	0.14	1.50
$^{238}U+^{181}Ta$	6.30	W3	0.34	1.64

equal. In the laboratory frame, the individual energies are kinematically shifted but, for a slowly moving source, these shifts approximately cancel in the laboratory and result in pairs with a sharp sum energy, and a small energy difference $\Delta E = E(e^+) - E(e^-)$. Such events lie in an approximately wedge-shaped region located symmetrically around the diagonal in the two-dimensional space of positron-electron energies. For $\beta_{\text{source}} = \beta_{\text{c.m.}}$ (the center-of-mass velocity of the collision system), this wedge is defined by $0.80E_+ < E_- < 1.25E_+$. In the analysis of previous experiments [18] this selection, referred to as a "wedge cut," was slightly asymmetric $(0.75E_+ < E_- < 1.25E_+)$.

Other, empirically motivated wedge cuts, not symmetric about the $E(e^+) = E(e^-)$ diagonal were also used in previous studies [21]. These cuts were introduced mainly to eliminate backgrounds in the sum-energy spectrum arising from the numerous low-energy electrons. Such a selection might also be appropriate in enhancing the sensitivity of the analysis to scenarios such as IPC where, due to Coulomb repulsion, the positron receives on average more energy than the electron. We have applied such selections to our data. The parameters summarizing the wedge cuts used in our analysis are given in Table III.

2. Angle selection

Another class of event selection is based on the angles of emission of the positron and electron. To search for pairs with kinematic behavior consistent with the decay of a slowly moving neutral object, we first use only the angular information taken from the azimuthal segmentation of the silicon arrays. In this analysis, pairs with the electron (positron) detected in a silicon-array element 180° away in ϕ from the element in which the positron (electron) was identified ($\Delta\phi_{+-} \approx 180°$), and with difference energies ΔE consistent with the expected shifts for a slowly moving ($\beta < 0.05$) source, are selected. Further, only pairs in which the positron and electron are detected in opposite arms of the spectrometer are included, enhancing the sensitivity to the angular correlation expected for neutral particle decay. This analysis was referred to as "the particle analysis" in Ref. [25]. This procedure does not use the polar angle information in APEX, but is, nevertheless, sufficient to eliminate $\approx 95\%$ of the pairs whose kinematic behavior is inconsistent with particle decay [38]. To restrict further the events to those

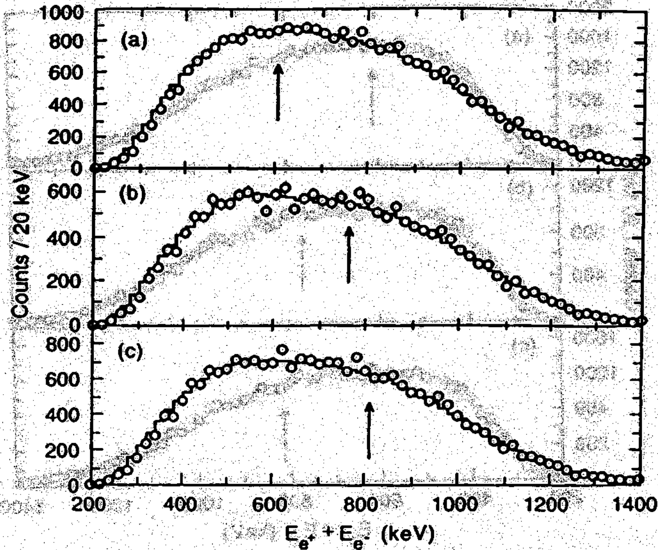

FIG. 14. Positron-electron sum-energy spectra from $^{238}U+^{232}Th$ collisions obtained for wedge cuts associated with previously reported sum-energy lines at (a) 608 keV (W1), (b) 760 keV (W2), and (c) 809 keV (W3). The solid lines represent the spectra obtained from event mixing. The arrows indicate the positions of previously observed sum-energy lines.

with kinematic behavior which most closely conforms to that of particle decay, we have also selected events based on the pair opening angle, using both the polar and azimuthal angle information from APEX.

B. $^{238}U+^{232}Th$

Previous results for the $^{238}U+^{232}Th$ system have attracted a great deal of attention. In Ref. [18], a peak consistent with the expectations for the decay of a light neutral particle was observed at $E_{e^+} + E_{e^-} = 760$ keV. Subsequent measurements by the same group [21] also identified structures at $E(e^+) + E(e^-) = 608$ keV and 809 keV, but the 760 keV peak was not observed (see Table I). We have used the wedge cuts described in Table III to search for these peaks. Pair peaks arising from neutral particle decay have been investigated using other cuts on the data as described above. Finally, motivated by the suggestion [29] that significant effects may exist in our data at a level lower than that reported in [18,21], we carried out several other similar analyses of our data, and in particular have studied the effects of small changes in the analysis procedure on the results.

1. Wedge cuts

The sum-energy spectra obtained from our data following the wedge cuts described in Refs. [18,20–22] are shown in Fig. 14(a)–(c). Here, to enhance the sensitivity to particlelike decays, only positrons and electrons detected in opposite spectrometer arms were included. The previously reported line structures [18,20–22] are not apparent in these spectra. Superimposed on the data, in each case, is the continuum spectrum obtained from adding the energy of a positron from one event to that of electrons from different events ("event

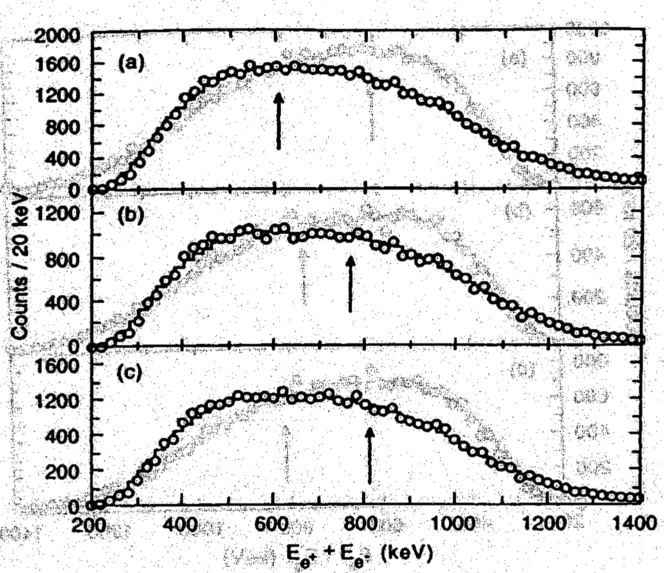

FIG. 15. Same as Fig. 14 except with electron positron pairs from all combinations of spectrometer arms.

mixing''). This procedure provides a reference shape of the sum-energy spectrum from uncorrelated positron-electron pairs. The normalization of this continuum to the data is fixed and is given only by the number of mixed pairs used to generate the uncorrelated sample. In every case, the data are well described by the assumption that the positron and electron energies are completely uncorrelated, with values of the reduced χ^2_ν of 1.16, 1.48, and 1.35 for the results shown in Figs. 14(a), (b), and (c), respectively. For the case in which the positron and electron have no preferred angular correlation, the results appear in Fig. 15, which shows the data analyzed in the same manner as in Fig. 14, except that positron-electron pairs from all combinations of spectrometer arms are included. The uncorrelated continuum is again in reasonable agreement with the data, although the reduced χ^2_ν values of 1.89, 2.49, and 2.12 for (a), (b), and (c) are slightly larger than those for the data in Fig. 14. In general, the deviations from the event-mixed background are largely at low sum energies, where contributions from correlated pairs from IPC, and events containing misidentified positrons, are concentrated.

The 90% (1.65σ) confidence level upper limits for the presence of lines in our data are summarized in Table IV. For the ^{238}U+^{232}Th system, the limits for peaks at sum energies of 608, 760, and 809 keV, derived from our data, are $d\sigma/d\Omega_{HI}<0.14$, 0.11, and 0.12 μb/sr, respectively, assuming a back-to-back angular correlation between the positron and electron. The quantity $d\sigma/d\Omega_{HI}$ is the differential cross section for line production per unit of heavy-ion solid angle. For comparison, a signal with a strength of 0.50 μb/sr would correspond to a peak with an intensity of approximately 400 counts in the spectrum of Fig. 14(a), distributed over two channels. In the case of the lines at 608 and 809 keV, these limits are a factor of 5 to 10 smaller than the corresponding cross sections for pairs with a back-to-back geometry from Refs. [20,21], as analyzed by Ganz *et al.* [23]. For the line at 760 keV, no previous value is available, although Ref. [18] reports that the observed peak yield was consistent with the cross section of the singles lines, i.e., between 5–10 μb/sr.

TABLE IV. Summary of APEX experimental upper limits for lines from e^+-e^- coincidences.

System	Beam energy (MeV/nucleon)	Sum energy (keV)	Upper limit (90% C.L.) $d\sigma/d\Omega_{HI}$(μb/sr) (iso)[a]	(bb)[b]
^{238}U+^{232}Th	5.78–5.95	608	0.26	0.14
^{238}U+^{232}Th	5.78–5.95	760	0.21	0.11
^{238}U+^{232}Th	5.78–5.95	810	0.23	0.12
^{238}U+^{181}Ta	5.78–5.95	625	0.20	0.14
^{238}U+^{181}Ta	5.94–6.10	625	0.19	0.12
^{238}U+^{181}Ta	6.13–6.30	625	0.34	0.23
^{238}U+^{181}Ta	5.78–5.95	748	0.25	0.18
^{238}U+^{181}Ta	5.94–6.10	748	0.24	0.16
^{238}U+^{181}Ta	6.13–6.30	748	0.42	0.29
^{238}U+^{181}Ta	5.78–5.95	805	0.20	0.14
^{238}U+^{181}Ta	5.94–6.10	805	0.19	0.12
^{238}U+^{181}Ta	6.13–6.30	805	0.34	0.23
^{238}U+^{181}Ta	5.78–5.95	635	0.13	—
^{238}U+^{181}Ta	5.94–6.10	635	0.13	—
^{238}U+^{181}Ta	6.13–6.30	635	0.24	—

[a]Upper limit obtained assuming no e^+-e^- angular correlation.
[b]Upper limit obtained assuming pair kinematics consistent with particle decay.

2. Wedge and angle cuts

Figure 16 shows the APEX ^{238}U+^{232}Th pair sum-energy spectra for energy and angle cuts appropriate to the particle hypothesis. For comparison, Fig. 14(b) shows the sum-energy spectrum arising from a wedge cut corresponding to a source velocity of $\beta_{\rm c.m.}$. The events remaining after imposition of the $\Delta\phi_{+-}\approx 180°$ cut are shown in Fig. 16(a). Based on Monte Carlo simulations, in ''signal'' to background, an improvement of approximately a factor of 10 is expected [38]. The corresponding event-mixed spectrum shows good overall agreement with the data, with a reduced χ^2_ν value of 1.18 for the fit. The magnitude of the fluctuations observed in Fig. 16(a) shows the sensitivity of this analysis to weak structures, and corresponds to production cross sections of between 0.01 and 0.02 μb/sr.

Figure 16(b) shows the sum-energy spectrum obtained with the particle wedge cut combined with a requirement that the opening angle between the positron and electron be greater than 150°. This angular range reflects the expected opening-angle resolution for near back-to-back events. The event-mixed spectrum also reproduces the measured one well, with $\chi^2_\nu=1.19$. The upper limits (90% C.L., 1.65 σ) on the cross section for a peak at 760 keV obtained from these two analyses, are considerably smaller than the limits obtained from the simple wedge-cut analyses, and are $d\sigma/d\Omega_{HI}\leq 0.02$ and 0.03 μb/sr, for the analysis of Figs. 16(a), and (b), respectively.

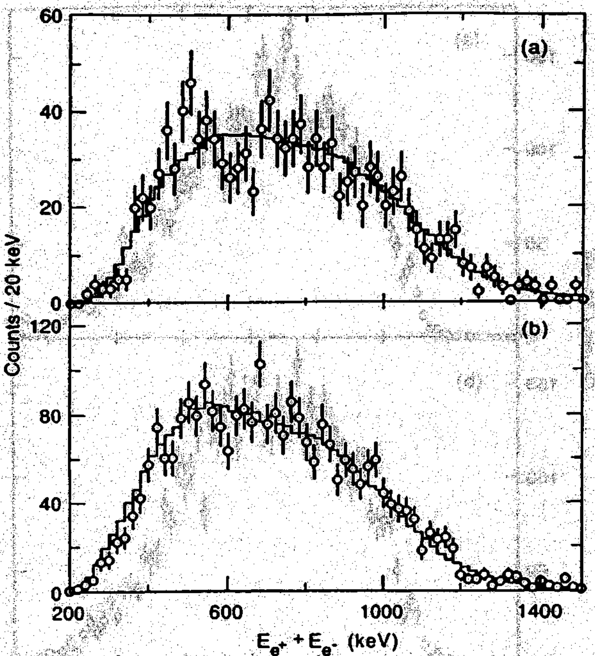

FIG. 16. Positron-electron sum-energy spectra obtained with a wedge cut appropriate for the 760 keV line, with additional restrictions on (a) the azimuthal angle difference, (b) the calculated opening angle, as described in the text. The solid lines represent the spectra obtained from event mixing.

We have also calculated the invariant mass spectrum for positron-electron pairs emitted from $^{238}U+{}^{232}Th$ collisions, which is shown in Fig. 17. Here, only events in which the positron and electron were detected on opposite arms of the spectrometer were included, enhancing the signal-to-background ratio for the back-to-back angular correlation expected for neutral-object decay. No significant structure is apparent. The cross-section limits for particles of mass near 1800 keV/c^2 are comparable to those from the wedge-cut analyses, but do not require the assumption of $\beta_{\mathrm{source}} = \beta_{\mathrm{c.m.}}$.

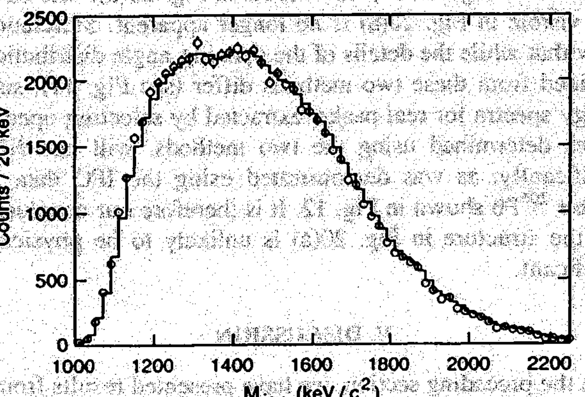

FIG. 17. Positron-electron invariant mass spectrum for pairs detected on opposite spectrometer arms, with no additional restriction on the lepton energies or angles.

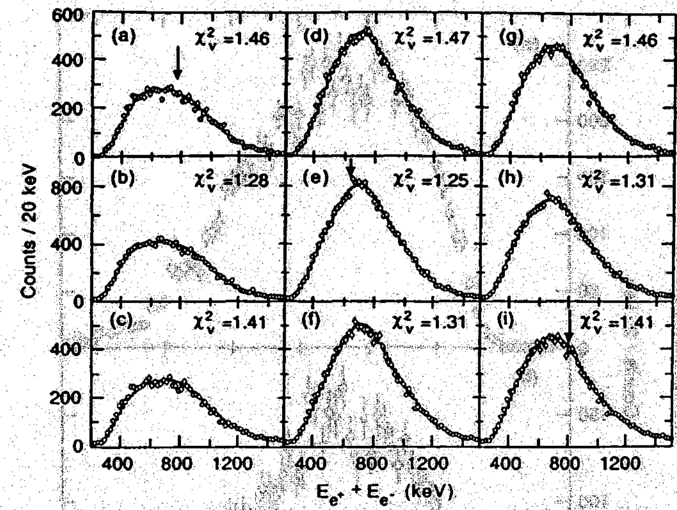

FIG. 18. Positron-electron sum-energy spectra from $^{238}U+{}^{181}Ta$ collisions at 5.95 MeV/nucleon (a),(d),(g), 6.1 MeV/nucleon (b),(e),(h), and 6.3 MeV/nucleon (c),(f),(i), obtained under the "wedge cut" conditions described in the text: W1 (a),(b),(c), W2 (d),(e),(f), and W3 (g),(h),(i). The points are the measured data, and the histograms are the uncorrelated background obtained from event mixing. The arrows in (a), (e), and (i) indicate the energies of previously reported sum-energy lines. The value of χ^2_ν for the agreement between the event-mixed background and the data is given in each panel.

C. $^{238}U+{}^{181}Ta$

For the $^{238}U+{}^{181}Ta$ system, the previously observed lines [21,23] had suggested characteristics which were different from those expected for a decaying particle. Also, the lines appeared at different bombarding energies, with different sum energies, when different wedge cuts were applied to the data, as listed in Tables I and III. We have applied these same wedge cuts to our $^{238}U+{}^{181}Ta$ data at each beam energy. Since the lines did not appear to arise from particle decay and had no preferred positron-electron angular correlation, all angle combinations were included in our analysis. Figure 18 shows positron-electron sum-energy spectra from our data at three beam energies, analyzed with the three different wedge cuts. Shown with the data are event-mixed histograms which well reproduce the experimentally measured shapes. The values of χ^2_ν for the spectra shown in Fig. 18 are all less than 1.50. As before, the deviations from the uncorrelated background are concentrated at low sum energies. In no case is there statistically significant evidence for the previously observed narrow structures.

Upper limits on the cross sections for such structure were also calculated as discussed in Ref. [39]. In these calculations, we assume that the peak width is consistent with our experimental resolution ($\Delta E_{\mathrm{sum}}=30$ keV) and with no preferred angular correlation of the positron-electron pair, and isotropic positron emission. Our upper limits (90% C.L., 1.65 σ) on the total production cross section for lines at the relevant energies are all less than 0.5 μb/sr, and are listed in Table IV. For comparison, the corresponding cross sections from previous experiments [20,21] as presented by Ganz *et al.* [23] are between 3 and 6 μb/sr, depending on the

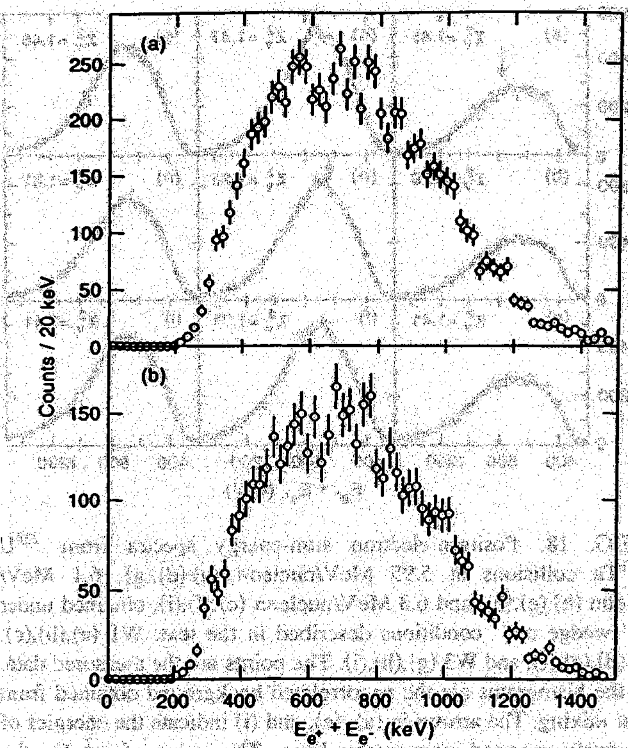

FIG. 19. Positron-electron sum-energy spectra for pairs produced in $^{238}U+^{232}Th$ collisions analyzed with wedge plus opening angle described in the text, and with (a) no restriction on the number of electrons in the event and (b) only events in which one electron is detected.

assumed positron-electron angular correlation.

D. Searches for weak structure

Although the present results are inconsistent with the presence of peaks of the strength seen in the earlier experiments, it is useful to search for weaker structure, in case there could still be interesting phenomena in our data. A particularly interesting result, based on an analysis of the present data for $^{238}U+^{232}Th$ collisions [29], suggests that, under particular conditions, significant structure may be present in the positron-electron sum-energy spectra. We have studied this possibility which, if substantiated, could yet represent a manifestation of the effects seen in the earlier experiments.

In the analysis of the present data presented in Ref. [29], a number of cuts, not well justified by physical scenarios, were applied to the data. For example, those events for which the electron fold was greater than one were rejected, to reduce the effects of backscattering in the measured spectra. As discussed in Sec. III B, and as shown in Fig. 6, the probability of a single electron resulting in two hits is at most 15%, but generally much smaller, and the majority of multiple-hit events result from the large ($M_{e^-}=4-5$) electron multiplicity. Sum-energy spectra from the wedge-cut plus opening-angle analysis for (a) all events and (b) events in which there was a single electron hit are shown in Fig. 19. The reduction of low-energy events in (b) expected if the single-hit requirement was reducing backscattering and thus

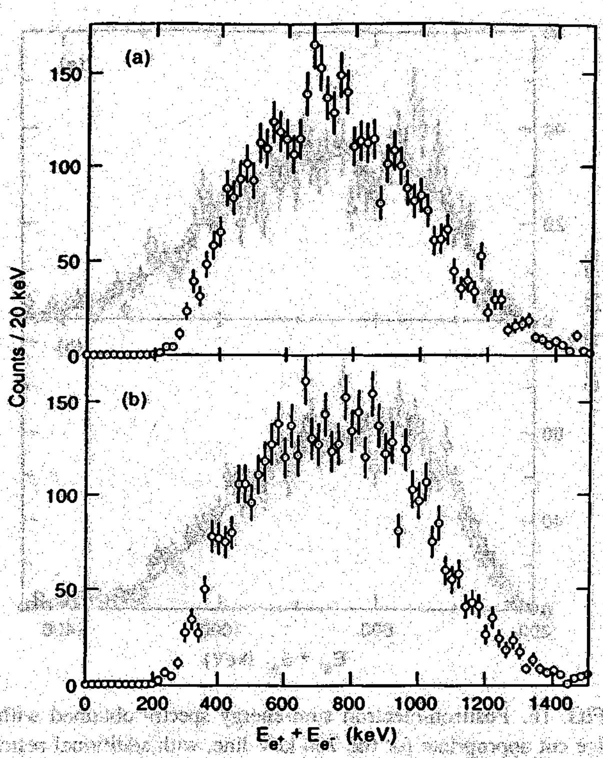

FIG. 20. Positron-electron sum-energy spectra analyzed (a) as suggested in Ref. [29], and (b) similarly analyzed with small modifications of the analysis as described in the text.

enhancing full-energy deposition events is not evident.

Other features of the analysis of Ref. [29] have no clear physical justification but do relate directly to the appearance of structure. Specifically, these include the method used in the opening-angle calculation. Figure 20 shows a repetition by us of the analysis reported in Ref. [29] using the same data set. As expected, this spectrum reproduces the one shown in Ref. [29]. The "structure" is the apparent excess of events in the energy range between 680 and 800 keV. This spectrum was obtained using opening angles calculated from discrete time-of-flight and discrete ϕ measurements as discussed in Sec. III D. The same data analyzed in an identical fashion except using opening angles calculated from continuous time of flight and ϕ are shown in Fig. 20(b). The structure visible in Fig. 20(a) is no longer apparent. Simulations show that while the details of the opening-angle distributions obtained from these two methods differ (see Fig. 11), sum-energy spectra for real peaks, extracted by selecting opening angles determined using the two methods, will not differ significantly, as was demonstrated using the IPC data for $^{206}Pb+^{206}Pb$ shown in Fig. 12. It is therefore our conclusion that the structure in Fig. 20(a) is unlikely to be physically significant.

V. DISCUSSION

In the preceding section, we have presented results from a variety of analyses of the APEX data based on different scenarios, both physical and empirical, for the origins of the previously reported sum-energy lines. None of these analyses provide positive evidence for lines at the previously reported energies, or any statistically convincing evidence for sharp sum-energy lines anywhere. Our results provide upper limits for the cross sections averaged over the bombarding energy range corresponding to the energy loss of the incident beam in our targets. Given our results, the question then is, to what extent are these upper limits inconsistent with previous results.

An effect which could influence the comparison between the experiments is an energy dependence of the line-production cross sections over the energy range corresponding to the target thickness. This variation could result in a target-thickness dependence of the yields and the derived cross sections. Some evidence for such an energy dependence is given in Ref. [21] which shows an excitation function for the ^{238}U+^{181}Ta 748 keV line. This line is only evident at bombarding energies between 5.93 and 6.16 MeV/nucleon, but not above or below this range. In these measurements [20,21], the thickness of the target corresponded to an energy loss of 0.10 MeV/nucleon. This result can be interpreted as a resonancelike behavior of the line cross section with a width of approximately 0.15 MeV/nucleon.

The situation is less clear for the other ^{238}U+^{181}Ta and the ^{238}U+^{232}Th sum-energy lines. It was reported that the cross sections for these lines may vary extremely rapidly with energy—perhaps over a range smaller than the target thickness used in the measurements. No quantitative information is available, however, beyond the observation that the lines were only observed over certain narrow ranges of bombarding energy. In any case, the experimentally deduced values must represent the cross section averaged over the target thickness.

A comparison of the bombarding energy ranges, including energy loss in the target, over which the lines were previously observed and the energy ranges covered by the APEX measurements is shown in Fig. 21. The maximum possible increase in our upper limits due to such possible target-thickness effects is a factor of 2.4, the ratio of the target thicknesses used in the different experiments. The APEX limits are in disagreement with the previous cross-section values even with such a factor. This point was the subject of a Comment [40] to Ref. [25], and our reply [26].

Two other experiments have also reinvestigated these questions. Both report negative results in searches for the peak phenomenon. Measurements with an upgraded version of the apparatus (EPOS) used in Refs. [18,20,21] were carried out for the ^{238}U+^{181}Ta and ^{238}U+^{232}Th systems, over a range of bombarding energies and with target thicknesses comparable to those used in the original experiments [23]. Although the original experimental conditions were reproduced as precisely as possible with improved apparatus, no evidence was found for sharp sum-energy lines. The upper limits obtained are comparable to the APEX results. Similarly, new measurements for the ^{238}U+^{181}Ta system using the apparatus of Refs. [9,10] (ORANGE) also led to negative results [24].

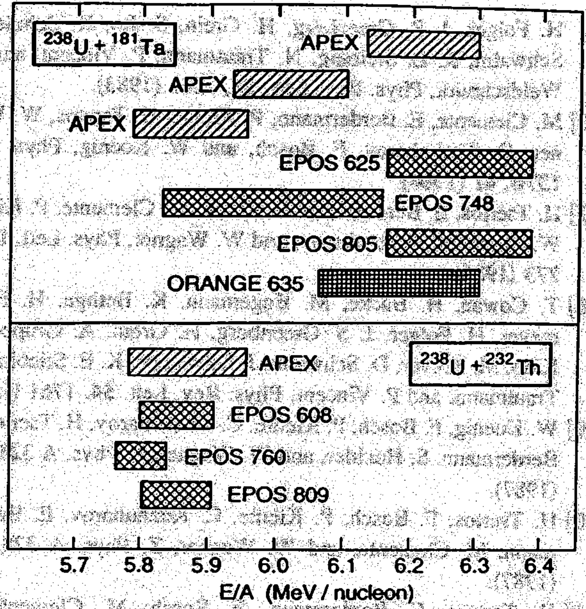

FIG. 21. Energies covered by various experiments reporting e^+-e^- coincidence lines in heavy-ion collisions.

In summary, the present experiments have provided no evidence for the previously reported lines in positron-electron sum-energy spectra measured for the ^{238}U+^{232}Th and ^{238}U+^{181}Ta systems. The upper limits for the line cross sections obtained from our data are, in all cases, significantly smaller than the values from the experiments reporting positive results, even when the effects of a possible energy dependence of the cross section are considered. This new body of evidence must call into question the significance of the earlier, positive, results.

ACKNOWLEDGMENTS

This work was supported by the U.S. Department of Energy, the U.S. National Science Foundation, and the Natural Sciences and Engineering Research Council of Canada. The work of the Argonne National Laboratory Physics Division is supported by the U.S. Department of Energy, Nuclear Physics Division, under Contract No. W-31-109-Eng-38. One of us (T.H.) acknowledges travel support from NATO Collaborative Research Grant No. 5-2-05 RG 910990.

[1] *Quantum Electrodynamics of Strong Fields*, edited by W. Greiner (Plenum Press, New York, 1983).

[2] *Quantum Electrodynamics of Strong Fields*, edited by W. Greiner, B. Müller, and J. Rafelski (Springer, Berlin, 1985).

[3] H. Backe, L. Handschug, F. Hesseberger, E. Kankeleit, L. Richter, G. Weik, R. Willwater, H. Bokemeyer, P. Vincent, Y. Nakayama, and J. S. Greenberg, Phys. Rev. Lett. **40**, 1443 (1978).

[4] C. Kozhuharov, P. Kienle, E. Berdermann, H. Bokemeyer, J. S. Greenberg, Y. Nakayama, P. Vincent, H. Backe, L. Handschug, and E. Kankeleit, Phys. Rev. Lett. **42**, 376 (1979).

[5] J. Schweppe, A. Gruppe, K. Bethge, H. Bokemeyer, T. Cowan,

H. Folger, J. S. Greenberg, H. Grein, S. Ito, R. Schule, D. Schwalm, K. E. Steibing, N. Trautmann, P. Vincent, and M. Waldschmidt, Phys. Rev. Lett. **51**, 2261 (1983).
[6] M. Clemente, E. Berdermann, P. Kienle, H. Tsertos, W. Wagner, C. Kozhuharov, F. Bosch, and W. Koenig, Phys. Lett. **137B**, 41 (1984).
[7] H. Tsertos, E. Berdermann, F. Bosch, M. Clemente, P. Kienle, W. Koenig, C. Kozhuharov, and W. Wagner, Phys. Lett. **162B**, 273 (1985).
[8] T. Cowan, H. Backe, M. Begemann, K. Bethge, H. Bokemeyer, H. Folger, J. S. Greenberg, H. Grein, A. Gruppe, Y. Kido, M. Klüver, D. Schwalm, J. Schweppe, K. E. Stiebing, N. Trautmann, and P. Vincent, Phys. Rev. Lett. **54**, 1761 (1985).
[9] W. Koenig, F. Bosch, P. Kienle, C. Kozhuharov, H. Tsertos, E. Berdermann, S. Huchler, and W. Wagner, Z. Phys. A **328**, 129 (1987).
[10] H. Tsertos, F. Bosch, P. Kienle, C. Kozhuharov, E. Berdermann, M. Clemente, and W. Wagner, Z. Phys. A **328**, 499 (1987).
[11] H. Tsertos, E. Berdermann, F. Bosch, M. Clemente, S. Huchler, P. Kienle, W. Koenig, and C. Kozhuharov, Z. Phys. A **342**, 79 (1992).
[12] B. Müller, in *Physics of Highly Ionized Atoms*, edited by R. Marrus (Plenum, New York, 1989), p. 39.
[13] E. M. Riordan, M. W. Krasny, K. Lang, P. de Barbaro, A. Bodek, S. Dasu, N. Varelas, X. Wang, R. Arnold, D. Benton, P. Bosted, L. Clogher, A. Lung, S. Rock, Z. Szalata, B. W. Fillipone, R. C. Walter, J. D. Bjorken, M. Crisler, A. Para, J. Lambert, J. Button-Shafer, B. Debebe, M. Frodyma, R. S. Hicks, G. A. Peterson, and R. Gearhart, Phys. Rev. Lett. **59**, 755 (1987).
[14] H. Tsertos, C. Kozhuharov, P. Armbruster, P. Kienle, P. Krusche, and K. Schreckenbach, Phys. Lett. B **207**, 273 (1988).
[15] H. Tsertos, P. Kienle, S. M. Judge, and K. Schreckenbach, Phys. Lett. B **266**, 259 (1991).
[16] X. Y. Wu, P. Asoka-Kumar, J. S. Greenberg, S. D. Henderson, H. Huomo, K. G. Lynn, M. S. Lubell, R. Mayer, J. M. McDonough, B. F. Philips, and A. Vehanen, Phys. Rev. Lett. **69**, 1729 (1992).
[17] S. D. Henderson, P. Asoka-Kumar, J. S. Greenberg, K. G. Lynn, S. McCorkle, J. McDonough, B. F. Philips, and M. Weber, Phys. Rev. Lett. **69**, 1733 (1992).
[18] T. Cowan, H. Backe, K. Bethge, H. Bokemeyer, H. Folger, J. S. Greenberg, K. Sakaguchi, D. Schwalm, J. Schweppe, K. E. Stiebing, and P. Vincent, Phys. Rev. Lett. **56**, 444 (1986).
[19] W. Koenig, E. Berdermann, F. Bosch, S. Huchler, P. Kienle, C. Kozhuharov, A. Schröter, S. Schuhbeck, and H. Tsertos, Phys. Lett. B **218**, 12 (1989).
[20] P. Salabura, Ph.D. thesis, Jagiellonian University, Krakow, 1989 GSI-Darmstadt, Report No. GSI-90-06, 1990.
[21] P. Salabura, H. Backe, K. Bethge, H. Bokemeyer, T. E. Cowan, H. Folger, J. S. Greenberg, K. Sakaguchi, D. Schwalm, J. Schweppe, and K. E. Stiebing, Phys. Lett. B **245**, 153 (1990).
[22] I. Koenig, E. Berdermann, F. Bosch, P. Kienle, W. Koenig, C. Kozhuharov, A. Schroter, and H. Tsertos, Z. Phys. A **346**, 153 (1993).
[23] R. Ganz *et al.*, Phys. Lett. B **389**, 4 (1996).
[24] U. Leinberger, E. Berdermann, F. Heine, S. Heinz, O. Joeres, P. Kienle, I. Koenig, W. Koenig, C. Kozhuharov, M. Rhein, A. Schroter, and H. Tsertos, Phys. Lett. B **394**, 16 (1997).
[25] I. Ahmad *et al.*, Phys. Rev. Lett. **75**, 2658 (1995).
[26] I. Ahmad *et al.*, Phys. Rev. Lett. **77**, 2839 (1996).
[27] I. Ahmad *et al.*, Phys. Rev. C **55**, R2755 (1997).
[28] I. Ahmad *et al.*, Phys. Rev. Lett. **78**, 618 (1997).
[29] M. Zeller and J. Sandweiss, Science **275**, 1401 (1997).
[30] I. Ahmad *et al.*, Nucl. Instrum. Methods Phys. Res. A **370**, 539 (1996).
[31] M. R. Wolanski, S. J. Freedman, J. W. Dawson, W. N. Haberichter, K. C. Chan, A. A. Chisti, N. I. Kaloskamis, and C. J. Lister, Nucl. Instrum. Methods Phys. Res. A **361**, 326 (1995).
[32] D. J. Mercer, D. Mikolas, J. Yurkon, S. M. Austin, D. Bazin, S. Gaff, E. Kashy, D. Kataria, J. S. Winfield, R. R. Betts, D. J. Henderson, A. L. Hallin, M. Liu, and F. L. H. Wolfs, Nucl. Instrum. Methods Phys. Res. A **350**, 491 (1994).
[33] R. C. Pardo, B. E. Clift, P. Denhartog, D. Kovar, W. Kutschera, and K. E. Rehm, Nucl. Instrum. Methods Phys. Res. A **270**, 226 (1988).
[34] D. E. Roa, L. Wright, J. D. Fox, J. P. Greene, B. B. Back, and B. G. Nardi, Nucl. Instrum. Methods Phys. Res. A **368**, 307 (1996).
[35] D. E. Roa, Ph.D. thesis, Florida State University, 1997.
[36] P. Kienle, Annu. Rev. Nucl. Part. Sci. **36**, 605 (1986).
[37] K. C. Chan, Ph.D. thesis, Yale University, 1994.
[38] M. R. Wolanski, Ph.D. thesis, University of Chicago, 1995.
[39] J. J. Hernández *et al.*, Review of Particle Properties, Phys. Lett. B **239**, III.28 (1990).
[40] T. E. Cowan and J. S. Greenberg, Phys. Rev. Lett. **77**, 2838 (1996).